NJC

ROYAL SOCIETY OF CHEMISTRY

PAPER

View Article Online
View Journal | View Issue

Cite this: *New J. Chem.*, 2024, **48**, 17722

Zwitterionic dioxidovanadium(v) complexes containing fluorinated triphenylphosphonium ligands: structure and biomacromolecule studies†

Francisco Mainardi Martins, [a] Daniele Cocco Durigon, [bc] Otávio Augusto Chaves, [d] Rosely Aparecida Peralta, [c] Davi Fernando Back *[a] and Hernán Terenzi *[b]

Research on metallodrugs with biological properties remains at the forefront, focusing on the development of compounds that interact non-covalently with deoxyribonucleic acid (DNA) and possess the ability to cleave the double helix strands of this biomacromolecule. In this context, vanadium(v) imine complexes featuring a fluorinated triphenylphosphonium group, (3-formyl-4-hydroxybenzyl)tris(4-fluorophenyl)phosphonium chloride (**[AF]Cl**), were studied for their targeting and accumulation in mitochondria, in addition to their interactions and ability to cleave DNA. The solid-state structures of complexes **C1–C3** were elucidated using single-crystal X-ray diffraction and were characterized using vibrational techniques and elemental analysis, along with extensive characterization in solution. These studies revealed that the complexes contain *cis*-dioxidovanadium(v) species and are zwitterionic species. It was shown that **C1–C3** can interact with and are capable of cleaving plasmid DNA through oxidative mechanisms without the need for photoinduction. When potential interactions with bovine serum albumin were analyzed, it was revealed that interactions in the order of 10^4 M^{-1} (Stern–Volmer quenching constant, K_{SV}) were observed. Additionally, *in silico* molecular docking studies showed that **C1–C3** can preferentially interact with the minor grooves of DNA and with domain IB (site III) of bovine and human serum albumins.

Received 9th July 2024,
Accepted 26th September 2024

DOI: 10.1039/d4nj03087g

rsc.li/njc

Introduction

Interactions between small molecules and deoxyribonucleic acid (DNA) can be irreversible or reversible. In the first case, covalent bonds are formed, for example, when using platinum-based antitumor drugs.[1] The employment of these Pt-complexes, particularly cisplatin, leads to different and severe side effects[2,3] and also cases of chemoresistance.[4,5] The formation of covalent bonds with DNA represents the main drawback for the use of cisplatin.[6] Reversible recognition of nucleic acids involves non-covalent interactions and usually can be defined as intercalative, major/minor groove binding, and/or electrostatic interactions.[1] The development of compounds that interact in non-covalent and reversible ways with DNA targets is at the forefront of the synthesis of new antineoplastic metallodrugs.[6–8]

The cleavage of both strands of the DNA double helix is medically significant because it causes damage to cells, resulting in cell death.[9] Therefore, the study of complexes capable of cleaving the DNA chain at specific sites has garnered interest due to their potential contributions to genomics and their applications in photodynamic therapy and chemotherapy against neoplasms.[10,11]

Mechanistically, two major types of cleavage can occur, namely hydrolytic or induced by reactive oxygen species (ROS) and the last one being categorized into oxidative or photocleavage. Generally speaking, synthetic metallonucleases that cleave DNA through hydrolytic mechanisms typically feature metal ions with inert redox properties and strong Lewis acidity *via* a reversible reaction, whereas those with ROS-induced mechanisms usually occur *via* irreversible reactions involving redox-active metal ions or photosensitizers.[9,12,13] The interaction and cleavage of DNA by

[a] *Laboratory of Inorganic Materials, Department of Chemistry, CCNE, Federal University of Santa Maria, Santa Maria, RS, 97105-900, Brazil. E-mail: davi.f.back@ufsm.br*
[b] *Laboratory of Structural Molecular Biology, Department of Biochemistry, Federal University of Santa Catarina, Florianópolis, SC, 88040-900, Brazil. E-mail: hernan.terenzi@ufsc.br*
[c] *Laboratory of Bioinorganic and Crystallography, Department of Chemistry, Federal University of Santa Catarina, Florianópolis, SC, 88040-900, Brazil*
[d] *CQC-IMS, Department of Chemistry, University of Coimbra, Coimbra, 3004-535, Portugal*

† Electronic supplementary information (ESI) available. CCDC 2367124–2367126 for **C1–C3**. For ESI and crystallographic data in CIF or other electronic format see DOI: https://doi.org/10.1039/d4nj03087g

redox-active metal complexes are crucial for developing antineoplastic therapeutic compounds.[14] In this context, certain cations have garnered increased attention, such as manganese(III),[15] iron(III),[15] cobalt(II),[16] ruthenium(II),[17,18] and vanadium(IV/V).[19,20]

Vanadium is a redox-active transition metal abundantly dissolved in marine waters,[21] exhibiting ions in variable oxidation states,[22] with III, IV, and V being the most common and biologically relevant.[23,24] When tetra- or pentavalent, vanadium metal centers are often stabilized in their oxido ($[VO]^{2+}$ or $[VO]^{3+}$) or *cis*-dioxidovanadium (*cis*-$[VO_2]^{+}$) forms due to their high oxophilicities and Lewis acidity in these oxidation states.[25,26] Vanadium ions perform various biological functions,[27–29] such as constituting nitrogenase enzymes[30,31] and haloperoxidases.[32,33]

Several types of vanadium-containing compounds have been studied for their potential therapeutic properties,[34–36] including insulin-enhancing properties[37] (notably, complexes bis(maltolate)oxidovanadium(IV), BMOV, and bis(ethylmaltolate)oxidovanadium(IV), BEOV),[38,39] antibacterial,[40,41] antiviral,[42–44] antiparasitic,[45,46] and antineoplastic activities[47–49] (*e.g.*, bis(4,7-dimethyl-1,10-phenanthroline)sulfateoxidovanadium(IV), metvan).[50] In recent years, several vanadium(V) complexes containing different imine ligands have been synthesized and evaluated for their interactions with biomacromolecules, including serum albumins and DNA,[51–53] cytotoxic potential,[35,54–56] and/or photoinduced DNA cleavage.[57–59]

Recently, the focus on vanadium complexes has extended to specifically target mitochondria,[60] offering a potential strategy for effectively inducing tumor cell death. Mitochondria play key roles in cellular energy production and in the execution of cell death through apoptotic mechanisms. Therefore, the production of reactive oxygen species, mitochondrial changes, upregulation of anti-apoptotic factors, and the acquired inability of the tumor suppressor protein p53 to activate the pro-apoptotic proteins Bak and Bax connect this organelle to the formation and growth of neoplasms.[61]

For mitochondrial targeting of a compound of interest, derivatization with triphenylphosphonium groups (+TPP) has been a strategy employed by the pharmaceutical industry for years,[62] as these groups preferentially accumulate in the anionic mitochondrial matrix due to their cationic charge.[61] These groups, widely regarded as the ''gold standard'' for mitochondrial vectors, also exhibit high lipophilicity, exceptional stability under physiological conditions, and facile conjugation with the compound of interest.[63] Consequently, the potential for derivatizing +TPP groups with 4-fluoro substituents is assessed.

Fluorination of molecules is a prevalent step in modern medicinal chemistry aimed at developing compounds with enhanced metabolic stability, bioavailability, and protein interactions. Fluorine atoms can modulate lipophilicity and facilitate weak hydrogen bonds and electrostatic interactions in organofluorine compounds.[64] The unique physical and chemical characteristics of fluorinated compounds arise from the small atomic radius and high electronegativity of fluorine.[65] Significant advances in fluorinated drug development with varying properties have occurred in recent years, including antifungals and antivirals, as well as in antineoplastic therapies.[66]

This study reports the synthesis of (3-formyl-4-hydroxybenzyl)-tris(4-fluorophenyl)phosphonium chloride (**[AF]Cl**), along with its use as a building block in the synthesis, characterization, and biological applications of three new zwitterionic complexes of *cis*-dioxidovanadium(v) (**C1–C3**) containing imine hydrazone ligands (**[H_2L1]Cl–[H_3L3]Cl**). The structures of complexes **C1–C3** were elucidated by single-crystal X-ray diffraction and characterized by various techniques in solution and in the solid state. Concerning biologically relevant applications, these complexes were evaluated for their interactions and cleavage potentials with DNA and bovine serum albumin through gel electrophoresis assays, fluorescence and UV-vis spectroscopies, and also molecular docking studies.

Experimental

General characterization and instrumentation

All the spectra of the techniques used to characterize the chemical structure of the compounds under study are presented in Fig. S1–S48 in the ESI.†

The nuclear magnetic resonance (NMR) spectra of nucleus ^{1}H (600 MHz), ^{13}C (151 MHz), ^{19}F (565 MHz), ^{31}P (243 MHz), and ^{51}V (158 MHz) were recorded using a Bruker AVANCE III 600 MHz spectrometer at 25 °C. Dimethyl sulfoxide (DMSO-d_6) and chloroform ($CDCl_3$) were used as deuterated solvents. Tetramethylsilane (TMS, Me_4Si) was used as the internal reference, while trichlorideoxidovanadium(v) in deuterated benzene (90% $VOCl_3/C_6D_6$ solution), triphenylphosphane (PPh_3), and trifluorotoluene (CF_3Ph) were used as external references. Chemical shifts were reported in parts per million (δ, ppm) and were referenced to residual DMSO-d_6 or TMS ($CDCl_3$) peaks. The multiplicities were expressed as follows: s, singlet; d, doublet; t, triplet, and m, multiplet.

The Fourier-transform infrared (FT-IR) spectra in transmission mode were recorded using a Bruker Vertex 70 spectrometer equipped with an ATR diamond accessory in the 4000–30 cm^{-1} region with 64 scans and 4 cm^{-1} resolution. On the other hand, the Fourier-transform Raman (FT-Raman) spectra of the complexes (crystalline materials) in absorbance mode were recorded using a Bruker SENTERRA confocal Raman microscope. The scattered beam was collected using an Olympus 20× objective and the spectra were recorded in the 3500–50 cm^{-1} range with a laser line of 785 nm. The spectra were recorded at a power of 25 mW with 6 coadditions of 10 seconds each.

The mass spectra of the inorganic complexes were obtained using an Amazon ion trap mass spectrometer *via* electrospray ionization (ESI-MS). The analysis was carried out in an ultrapure acetonitrile solution at a concentration of 500 ppb at 180 μL min^{-1}. The capillary temperature was maintained at 180 to 200 °C and a voltage of −400 to −500 V. The simulated spectra were calculated using the mMass software.[67]

Finally, the electronic spectra in the UV-Vis region were obtained using a Varian Cary 50 BIO UV-vis spectrometer coupled to a thermostatic bath at 25 ± 1 °C, using *N,N*-dimethylformamide (DMF) as the solvent and a cuvette with 1.0 cm optical path.

Crystallography

Data were collected using a Bruker D8 Venture Photon 100 diffractometer equipped with an Incoatec IμS high brilliance Mo-Kα X-ray tube with two-dimensional Montel micro-focusing optics. Measurements were made at low temperature using a Cryostream 800 unit from Oxford Cryosystems. The structures were initially solved by the intrinsic phasing method using the XT/SHELXT program and refined with XL/SHELXL with anisotropic displacement factors for non-hydrogen atoms.[68] All refinements were made by full-matrix least-squares on F2 with anisotropic displacement parameters for all non-hydrogen atoms. The hydrogen atoms were included in the refinement in calculated positions but the atoms (of hydrogens) that are performing special bonds were located in the Fourier map. Drawings were done using ORTEP-3 2020.1 for Windows.[69,70] Crystal data and more details of the data collection/refinements of **C1–C3** are presented in Table S1 in the ESI.†

DNA binding and cleavage studies

In a typical experiment, the cleavage of plasmid DNA (pBSK-II) was initiated with 2 μL (330 ng DNA), and 2 μL of various buffers (10 mM) alongside 5 μL of the complexes, where concentrations ranged from 0 to 500 μM. To reach a total volume of 20 μL, 11 μL of ultra-pure water was added in an Eppendorf microtube. The reactions were conducted for various durations (8 or 16 hours) at an incubation temperature of 50 °C, shielded from light exposure. To stop the reactions, 5 μL of the sample buffer (0.25 M EDTA, pH 8.0, 50% glycerol, and 0.01% bromophenol blue) was introduced. The samples were subsequently stored at 4 °C until analysis *via* 1% agarose gel electrophoresis, which contained ethidium bromide (0.3 μg mL^{-1}) for 100 minutes at 90 V in TBE buffer (44.5 mM TRIS, 44.5 mM boric acid, and 1.00 mM EDTA, pH 8.0).

The gels were imaged and quantitatively analysed by densitometry using the ImageJ software. Given that ethidium bromide intercalates to a lesser extent with the supercoiled form of the plasmid DNA, a correction factor of 1.47 was applied when assessing this specific conformation of plasmid DNA.[71]

To determine the DNA interaction and cleavage preferences by the complexes, external agents were incorporated into the reaction mixtures. This included lithium perchlorate ($LiClO_4$, to augment the ionic strength of the reaction media) and minor-groove binders (4′,6-diamidino-2-phenylindole, DAPI, and netropsin, NET; 50 μM) along with a DNA major-groove binder (methyl green; 50 μM).

Studies on the interactions between the complexes and calf thymus DNA (ct-DNA, stock solution 1.0 mM) were conducted using a Varian Cary 50 Bio UV-vis spectrophotometer connected to a thermostatic bath maintained at 25 ± 1 °C. Complexes **C1–C3** were examined in a DMF/buffer (TRIS 0.5 mM) solution (5% v/v) at pH 7.40 and an ionic strength (*I*) of 0.5 mM (NaCl).

Protein binding and cleavage studies

The binding affinities of the complexes for proteins were investigated through their interactions with bovine serum albumin (BSA) using fluorescence spectroscopy. Tryptophan fluorescence quenching assays of BSA (2 μM) were performed in a solution (0.1 M TRIS–HCl buffer–0.1 M NaCl, pH 7.5) at room temperature. The emission spectra were monitored at 290–550 nm with excitation at 280 nm. Upon the incremental addition of complexes, fluorescence spectra were acquired after 5-minute incubation for each addition, utilizing a Cary Varian Eclipse spectrofluorometer at ambient temperature.

Molecular docking procedures

The crystallographic structure of DNA, BSA, and human serum albumin (HSA) was obtained from the Protein Data Bank with access codes of 1BNA,[72] 4F5S,[73] and 3JRY,[74] respectively. The chemical structure of compounds **C1–C3** was obtained from the experimental X-ray data described in this work. Molecular docking calculations were performed with the GOLD 2022.3 software (Cambridge Crystallographic Data Centre, Cambridge, CB2 1EZ, UK). Hydrogen atoms were added to the biomacromolecules following tautomeric states and ionization data inferred using the GOLD 2022.3 software at pH 7.4.

For the DNA structure, an 8 Å radius around the two main possible binding sites (major and minor grooves) was explored,[75] while for BSA and HSA, an 8 Å radius around the three main binding pockets (subdomains IIA, IIIA and IB – known as sites I, II, and III, respectively)[76,77] was defined and explored. For all biomacromolecules, the standard ChemPLP was used as the scoring function. Protein–ligand interaction profiler (PLIP) webserver (**https://plip-tool.biotec.tu-dresden.de/plip-web/plip/index**)[78] was used for the identification of protein–ligand interactions and the 3D-figures were generated using the PyMOL Molecular Graphics System 1.0 level software (Delano Scientific LLC software, Schrödinger, New York, NY, USA).[79]

Synthetic procedures

The complexes were synthesized through one-pot *in situ* (metal template) reactions. All the synthetic methodologies (Scheme 1) and spectroscopic data for starting materials, ligands **$[H_2L1]Cl$–$[H_3L3]Cl$**, and complexes **C1–C3** are detailed in Section S1 in the ESI.†

Results and discussion

Solid-state structures

The solid-state structures of the **C1–C3** complexes were elucidated by means of single-crystal X-ray diffraction, indicating their same coordination sphere; consequently, the solid-state structures of the complexes will be discussed collectively in a generalized manner. The ORTEP-3 crystallographic structural projections of complexes **C1–C3** in the solid state are depicted in Fig. 1. The values of selected bond lengths and angles for **C1–C3**, alongside similar complexes from the literature, are summarized in Tables S2 and S3 in the ESI.†

The complexes feature an iminic hydrazone ligand unity arising from the condensation of (3-formyl-4-hydroxybenzyl)tris-(4-fluorophenyl) chloride and the respective hydrazide, resulting

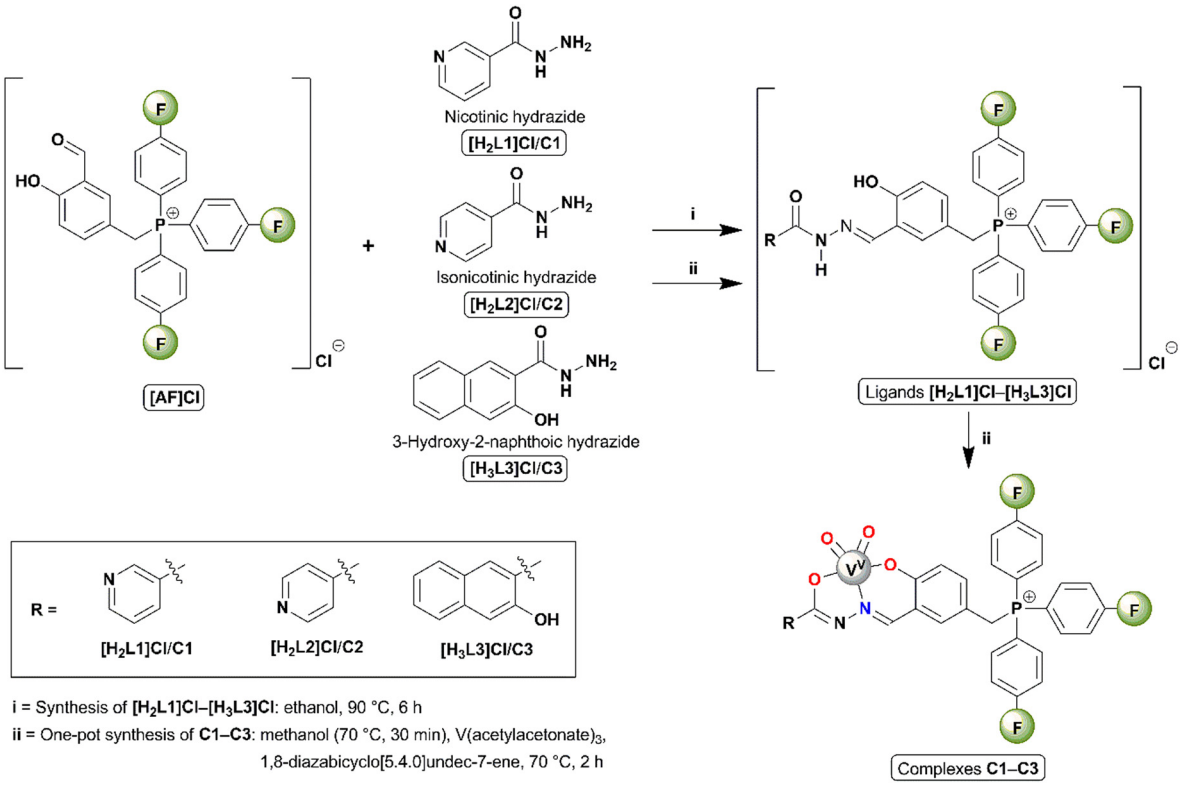

Scheme 1 General synthesis of ligands **[H$_2$L1]Cl–[H$_3$L3]Cl** and complexes **C1–C3**.

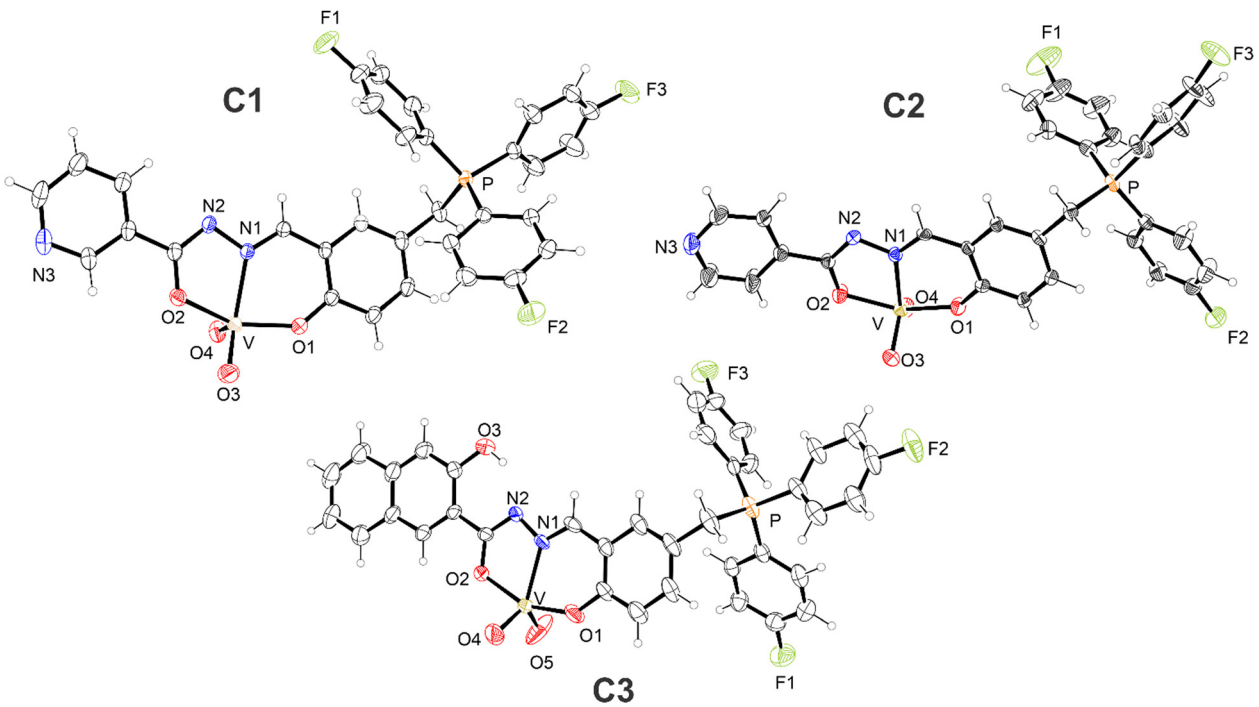

Fig. 1 ORTEP-3 crystallographic structural projections of complexes **C1**, **C2**, and **C3** in the solid state. Thermal ellipsoids are calculated with a 50% probability level. Crystallization solvates are omitted for better visualization.

in a tridentate chelating cavity that comprises phenol and carbonyl oxygens, and an iminic nitrogen as potential donor atoms for coordination.[80] However, the vanadium metal centers in **C1–C3** (mononuclear complexes) are coordinated to the

respective ligands through the anionic forms of such oxygen atoms. One is in the phenolate form (ranging from 1.898(5) to 1.915(2) Å) and the other is in the enolate form (ranging from 1.973(5) to 1.982(4) Å).

The enolate-form oxygen atom is generated by deprotonation of the amide nitrogen of the hydrazone moiety, as indicated by the bond lengths of C–N(amide) (ranging from 1.292(7) to 1.311(3) Å) and C–O(enolate) (ranging from 1.288(6) to 1.305(3) Å), and the C–N(amide)–N(imine) bond angles[81] (ranging from 108.1(2)° to 109.0(5)°) in **C1–C3**. Moreover, a neutral iminic nitrogen (ranging from 2.138(5) to 2.156(2) Å) acts as a third site in ligands characterized by an O,N,O tridentate dianionic motif. These values for **C1–C3**, along with the bond length values of their coordination spheres, bear similarities to those of selected complexes in the literature (Tables S2 and S3 in the ESI†).[82,83]

In addition to the ligand donor atoms, the vanadium metal centers in **C1–C3** coordinate with two oxido ligands (ranging from 1.588(6) to 1.646(2) Å), adopting the form of *cis*-dioxidovanadium (*cis*-$[VO_2]^+$), a distinctive species of vanadium(v). Consequently, **C1–C3** exhibit pentacoordinate coordination spheres. The geometries of **C1–C3** have been determined based on the values of the structural index parameter τ, calculated as $(\beta - \alpha)/60$, with β and α being, respectively, the largest and second largest bond angle values of the coordination spheres. The values of this parameter range from 0, representing a perfect square-based pyramid, to 1, denoting a perfect trigonal bipyramid. Non-integer values within this range indicate distorted geometries.[84] The β and α angles (°), calculated τ values (dimensionless), and coordination geometries of **C1–C3** are summarized in Table 1, with comparisons to some dioxidovanadium(v) complexes from the literature presented in Table S4 in the ESI.†[82,83]

Furthermore, given the sum of cationic and anionic charges, alongside the absence of counterions, these three complexes are classified as neutral zwitterionic complexes,[85] and this is due to the presence of the delocalized cationic charge intrinsic to the ligand of the tris(4-fluorophenyl)phosphonium group. This characteristic distinguishes them from the complexes reported by Maurya *et al.*[86,87] and Dash *et al.*,[57] wherein protonation and coordination of the pyridinic nitrogen atoms occur.

Spectroscopic characterization

The electronic UV-vis spectra of the dioxidovanadium complexes **C1–C3** (Fig. S45 of the ESI†) were recorded in DMF solution. For all three compounds, transition bands at 280–410 nm were revealed. The bands around 410 nm are best described as ligand-to-metal charge transfer (LMCT) from the phenolate ligand to the metal, while the other remaining and more energetic bands at 260–350 nm are attributed to intraligand transitions ($\pi \rightarrow \pi^*$ and $n \rightarrow \pi^*$).[88–90]

The stability of **C1–C3** in DMF/buffer – (TRIS 0.5 mM) 5% v/v; pH 7.40, I = 0.5 mM (NaCl) at 25 °C (Fig. S46–S48 of the ESI†) – was examined over 24 h using UV-vis absorption spectroscopy. The absorption spectra of all three compounds remained unchanged, indicating their stability and structural integrity during the investigated period.

DNA binding and cleavage studies

The agarose gel electrophoresis technique is employed to assess the DNA interaction properties of complexes using the plasmid DNA. The ability of vanadium(v) compounds to alter the supercoiled conformation of the pBSK-II plasmid DNA is observed through their electrophoretic mobility on agarose gels. This technique allows for the observation of two distinct DNA forms: the supercoiled circular form I and the open, singly nicked, circular form II.

Initially, the impact of pH on the reaction medium was assessed (Fig. 2). For all three complexes, a notable increase in DNA cleavage was observed at pH 6.0 and 7.0, after 8 hours of reaction at a complex concentration of 500 μM. Additionally, we noted that **C1–C3** exhibited similar activity. Consequently, pH 7.0 was selected for further assays.

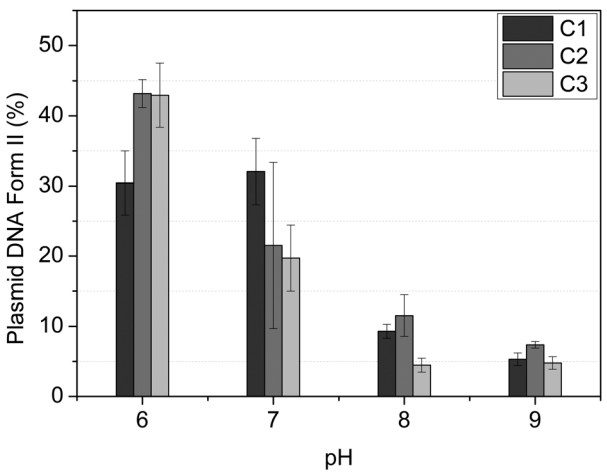

Fig. 2 pH effects on plasmid DNA cleavage. Experimental conditions: [DNA] = 330 ng, ≈25 μM; [buffer] = 10 mM, MES (6.0); HEPES (pH 7.0); HEPES (8.0); CHES (9.00); complexes concentration = 500 mM; temperature = 50 °C; incubation time = 8 hours sheltered from light.

Table 1 The β and α angles (°), calculated τ values (dimensionless), and coordination geometries of **C1–C3**

Complex	β angle[a] (°)	α angle[b] (°)	τ[c]	Coordination geometries[d]
C1	147.59(8)	145.77(11)	0.03	Slightly distorted SBP
C2[e]	155.46(17)/153.50(18)	125.6(2)/136.2(2)	0.50/0.29	Distorted between SBP and TB/distorted SBP
C3	154.9(2)	129.8(3)	0.42	Distorted between SBP and TB

[a] Highest bond angle value. [b] Second highest bond angle value. [c] Structural index parameter τ (dimensionless) calculated as $\tau = (\beta - \alpha)/60$. [d] SBP = square based pyramidal geometry and TB = trigonal bipyramidal geometry. [e] Two independent units of the complex in the asymmetric unit.

Notably, unlike similar compounds described by Dash and coworkers,[58,59] which involve mononuclear dioxovanadium(v) complexes containing aroylhydrazone derivative ligands and have shown DNA cleavage activity through photoinduced reactions, the compounds described herein, **C1–C3**, can cleave DNA in the absence of light and under mild pH conditions, specifically at pH 7.0.

The effect of complex concentrations was also investigated. For **C1–C3**, as shown in Fig. S52–S54 in the ESI,† it was possible to observe that the complexes exhibit a capacity to cleave DNA in a concentration-dependent manner at 500–30 μM. This demonstrates that increasing the concentration of the compound also increases its DNase activity.

The cleavage reaction was carried out in both aerobic and anaerobic environments, in a glovebox using argon as an inert gas. As shown in Fig. S55 in ESI,† the absence of oxygen significantly decreased the DNase activity of compounds **C1–C3**. Therefore, it can be inferred that the cleavage activity is dependent on oxidative processes. To obtain information on the preference for cleavage sites, the cleavage was investigated using DNA groove blockers, and the results of which are shown in Fig. S56 in the ESI.† Generally, complexes **C1–C3** showed an increase in DNA cleavage activity in the presence of minor groove binders, DAPI and NET, suggesting higher affinities of the vanadium complexes with the minor groove. Conversely, methyl green, a major groove binder, did not affect the DNase activity.

To comprehend the forms of interaction between the complexes and DNA, the impact of the ionic strength within the reaction medium was initially explored. We found that as the concentration of lithium perchlorate increased from 0 to 50 mM for all three complexes (Fig. 3 for **C1** and Fig. S57 and S58 in the ESI† for **C2** and **C3**, respectively); the cleavage of DNA by the complexes also exhibited a gradual decrease for all three complexes. Considering the negative charge of the DNA molecule at pH 7.0, this finding suggests that electrostatic interactions, probably the positive charge centered on the tris(4-fluorophenyl)phosphonium group, between the complex and DNA might play a role in their binding and subsequent cleavage.

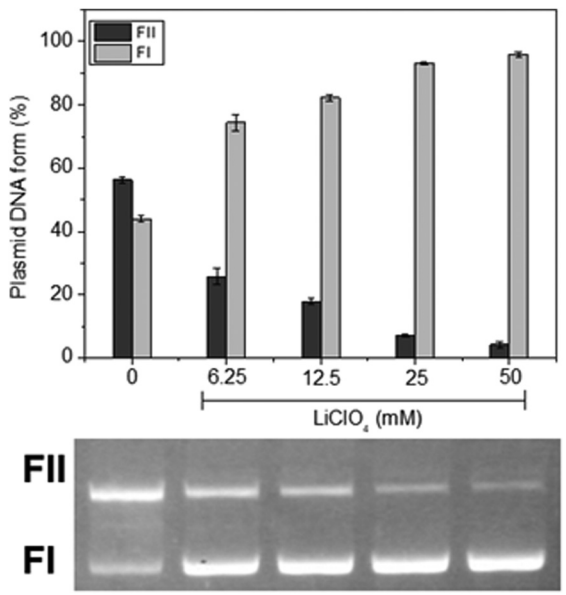

Fig. 3 Ionic strength effects on plasmid DNA cleavage for complex **C1**. Experimental conditions: [DNA] = 330 ng, ≈25 μM; [buffer] = 10 mM, HEPES (pH 7.0); complex concentration = 500 μM; temperature = 50 °C; incubation time = 16 hours sheltered from light.

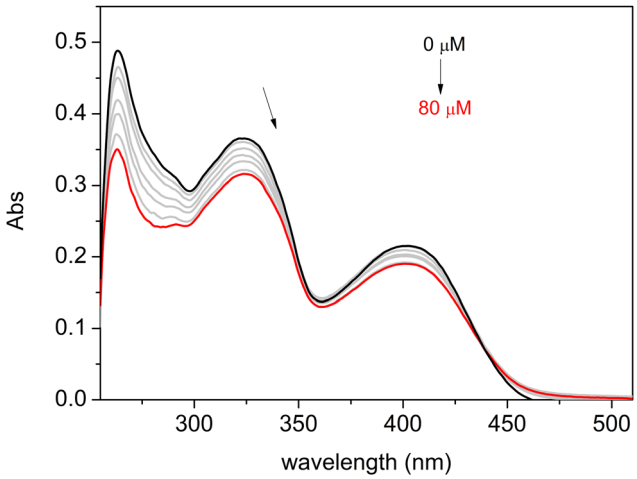

Fig. 4 Absorption spectra of complex **C3** on the titration of 0–80 μM ct-DNA in DMF/buffer (TRIS 0.5 mM) 5% v/v; pH 7.40, *I* = 0.5 mM (NaCl); 25 °C. An arrow indicates the changes in absorbance with the increasing concentration of ct-DNA.

The nature of the binding interaction between complexes **C1–C3** and ct-DNA was also examined using the UV-Vis absorption titration method, observing changes in absorbance and shifts in the wavelength of the complex spectra with increasing amounts of ct-DNA. The results are presented in Fig. 4 for **C3** and Fig. S59 and S60 in the ESI† for **C1** and **C2**, respectively. As a result, significant hypochromic changes were observed for all three compounds, along with slight bathochromic shifts.

In the absorption spectrum of a compound in the presence of DNA, changes such as hypochromism or hyperchromism and a wavelength shift (red or blue) frequently occur. Hypochromism and bathochromism (red shift) in UV-vis spectra are typically linked to the binding of a metal complex to DNA through intercalation involving π-stacking, van der Waals, and hydrophobic interactions between the metal complex and DNA.[91]

Protein binding studies

Serum albumin is the most abundant protein in the blood, transporting nutrients and drugs throughout the body.[92] More precisely, BSA is one of the most extensively studied protein models, with over 75% sequence similarity to human serum albumin and comparable drug-binding affinities.[93] Interaction studies between complexes **C1–C3** and BSA were conducted through steady-state fluorescence quenching assays at room temperature.

BSA fluorescence is primarily governed by the aromatic amino acid residues, namely tyrosine, phenylalanine, and

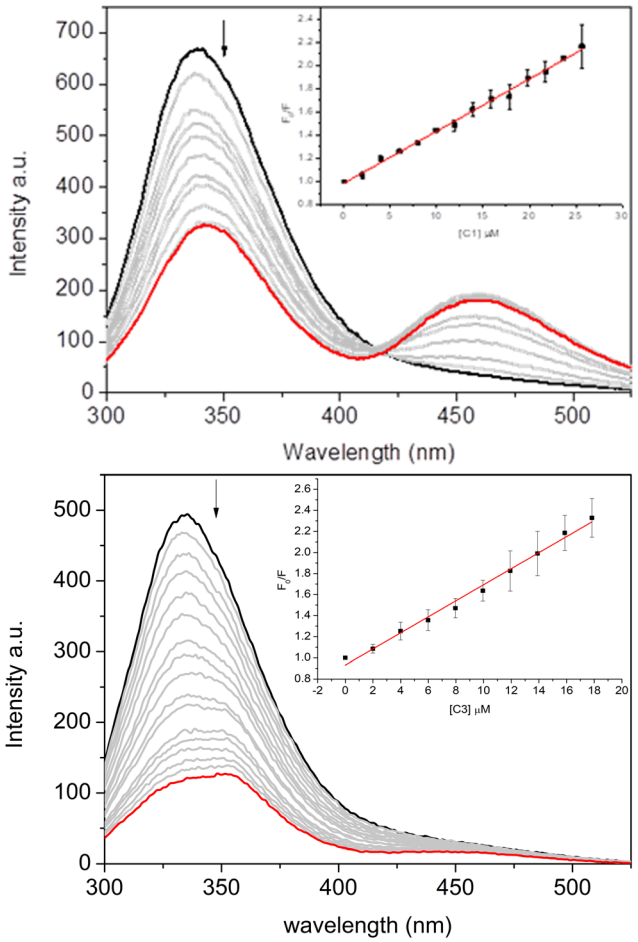

Fig. 5 Fluorescence spectra of BSA (2 μM) quenched by complexes **C1** (up) and **C3** (down) in the concentration range of 0–20 μM. Inset: The Stern–Volmer plot.

tryptophan (W134 and W213), with excitation at 280 nm. It is well-known that changes in the fluorescence behavior of albumin result from the interactions and/or changes in the microenvironment of these fluorophores caused by the quencher.[93]

Fig. 5 depicts the protein's maximum emission band at approximately 340 nm when excited at 280 nm. Observations from the steady-state fluorescence spectra revealed that an increase in the complexes' concentration (Fig. 5 for **C1** and **C3**, and Fig. S61 in the ESI† for **C2**) led to a significant decrease in the albumin's fluorescence intensity. This evidence suggests the binding between the complexes and the fluorophores of BSA.

An isosbestic point was also observed along with a new fluorescence band, indicating an increased fluorescence intensity in the 425–525 nm range. This phenomenon suggests the formation of an exciplex with BSA, which can be considered further evidence of more complex interactions between albumin and vanadium complexes.[94,95] This phenomenon was more evident for **C1** and **C2** than for **C3**, indicating the impact of the nicotinic and isonicotinic moieties on the spectroscopic signature of the binding of the inorganic complexes under study. Rio *et al.*[95] previously reported the capacity of albumin in forming exciplex in the presence of heterocyclic compounds (*e.g.*, 1,2,4-triazolo-3-thiones), highlighting the impact of the sulfide and sulfoxide groups.

To further explore these interactions, the Stern–Volmer quenching (K_{SV}) and binding (K_b) constants of the complexes were calculated and are summarized in Table 2. The Stern–Volmer equation is $F_0/F = 1 + K_{SV}[Q] = 1 + k_q\tau_0[Q]$, where F_0 and F represent the fluorescence intensity without and with the complexes, respectively, K_{SV} is the Stern–Volmer quenching constant, [Q] is the concentration of the complexes, k_q is the bimolecular quenching rate, and τ_0 is the fluorescence lifetime of BSA (6.06×10^{-9} s).[96] This calculation used corrected fluorescence data to account for the effect of dilution. The K_b values and the number of binding sites (n) were obtained from the Scatchard equation using double logarithm plots through the equation $\log(F_0 - F/F) = n\log[Q] + \log K_b$.

In Table 2, one can observe that the number of interaction sites for **C1–C3** is preferably one. The results (both K_{SV} and K_b) demonstrated that the binding constants of **C1** and **C2** are very similar, which is reasonable given their structural similarities. Conversely, compound **C3** exhibited the highest binding constant among the three complexes, reflecting the structural effects of incorporating naphthalenol as a pendant arm on the ligand. The values observed are in the same range or higher than those for similar [V^VO_2]-complexes reported in the literature, indicating that **C1–C3** might be distributed in the human bloodstream by the interaction with albumin.[26,52,59,97]

The bimolecular quenching rate constant (k_q) of all the complexes are larger than the diffusion rate constant in water ($k_{diff} \approx 7.40 \times 10^9$ M^{-1} s^{-1} at 298 K, following the Smoluchowski–Stokes–Einstein theory[98]), indicating a ground-state association.[99] The negative sign for the Gibb's free energy (ΔG), calculated based on the Van't Hoff equation ($\Delta G = -RT\ln K_b$, where R is the gas constant that is equal to 8.314 J mol^{-1} and T is the temperature in Kelvin), indicates that the binding process is spontaneous at 298.15 K.[100]

Table 2 BSA binding parameters of complexes **C1–C3**

Complex	$K_{SV}{}^a \times 10^4$ (M^{-1})	$k_q{}^b \times 10^{12}$ (s^{-1} M^{-1})	$K_b{}^c \times 10^4$ (M^{-1})	n^d	ΔG^e (kJ mol^{-1})
C1	4.48 ± 0.09	7.34	6.03 ± 0.13	1.03 ± 0.03	−27.28
C2	3.88 ± 0.07	6.36	7.76 ± 0.12	1.06 ± 0.02	−27.91
C3	7.62 ± 0.26	12.49	36.31 ± 0.18	1.22 ± 0.04	−31.73

[a] Stern–Volmer quenching constant. [b] Bimolecular quenching rate constant with BSA (τ = 6.06 ns). [c] Double logarithm binding constant. [d] Number of binding sites. [e] Gibbs free-energy values (R = 8.314 J mol^{-1} and T = 298.15 K).

Table 3 Molecular docking score values (dimensionless) for the interaction between DNA/BSA/HSA and complexes **C1–C3** in different binding sites

	DNA		Bovine serum albumin			Human serum albumin		
Complex	Major groove	Minor groove	Site I	Site II	Site III	Site I	Site II	Site III
C1	26.1	63.1	44.9	40.5	88.6	60.4	11.9	84.2
C2	32.1	65.1	41.4	25.2	84.9	59.0	7.76	87.8
C3	25.6	92.0	47.8	16.8	91.1	57.0	10.1	98.7

Molecular docking calculations for DNA and proteins

To offer a molecular point of view on the interaction between the $[V^{V}O_2]$-complexes and DNA/BSA/HSA, *in silico* calculations by the molecular docking approach were carried out at pH 7.4. Table 3 summarizes the docking score value (dimensionless) into the main binding pockets of DNA and serum albumins. Since each pose obtained using the GOLD 2022.3 software is considered as the negative value of the sum of energy terms from the mechanical-molecular type component, and more positive the docking score value indicates better interaction.

Thus, according to the computational results, for DNA which has two main binding sites (minor and major grooves), the $[V^{V}O_2]$-complexes fit preferentially into minor grooves than into major grooves (Table 3), agreeing with the experimental competitive binding assays. The same trend was previously *in silico* reported for the interaction between DNA and V^{V}-complexes derived from pyridoxal/salicylaldehyde.[52] On the other hand, BSA has three main binding pockets for both endogenous and exogenous compounds: subdomain IIA (site I) located in a hydrophobic binding pocket, subdomain IIIA (site II) also located in a hydrophobic binding pocket, and subdomain IB (site III) located on the surface of the protein.[101,102]

All binding sites were able to accommodate the $[V^{V}O_2]$-complexes; however, site III is the main pocket (Table 3) with docking score values close to 2-fold higher than for sites I and II. Interestingly, subdomain IB was not reported as the main binding site to V^{V}-complexes derived from pyridoxal or salicylaldehyde,[52,103] indicating dependence on the chemical nature of the ligands complexed with vanadium(v) species.

To verify if **C1–C3** will also have the same binding trend obtained from bovine to the human analogue, *in silico* calculations for HSA were also carried out and the results are summarized in Table 3. In this case, subdomain IB was also identified as the main binding site, reinforcing site III as the feasible cavity to the interaction of the $[V^{V}O_2]$-complexes. However, after a deep analysis of the docking score values, it is possible to note that BSA and HSA had practically the same score in site III, with differences in the other binding sites. This was expected due to the highest superposition of the 3D structure of the two proteins into subdomain IB compared to the other subdomains IIA and IIIA (Fig. 7A) with a global root mean square deviation (RMSD) value of 1.634 dimensionless. Interestingly, albumin-**C3** had the highest docking score value than albumin-**C1** or albumin-**C2**, following the same experimental binding trend.

In the case of DNA, molecular docking results suggested van der Waals interactions as the main intermolecular force responsible for the interaction with $[V^{V}O_2]$-complexes **C1–C3** (Table S5 in the ESI†), and despite the high steric volume of the inorganic complexes under study, they had good fit capacity in the double helix of DNA (Fig. 6) with the positive charge centered in the tris(4-fluorophenyl)phosphonium group of **C1–C3** close to the negative charged phosphate moieties of the DNA structure, agreeing with the experimental trend.

On the other hand, for BSA, interactions *via* hydrophobic, π-cation, and hydrogen bonding were suggested as the main binding forces, while for HSA hydrophobic interaction was detected and hydrogen bonding with π-stacking interaction was detected only for HSA-**C3** (Tables S6, S7 in the ESI† and Fig. 7). Interestingly, Dias *et al.*[104] reported that the interaction of the mixed species *cis*-[VO(carrier)$_2$-(HSA)] (carrier is picolinato, maltolato, or 3-hydroxy-1,2-dimethyl-4-pyridinone) involves

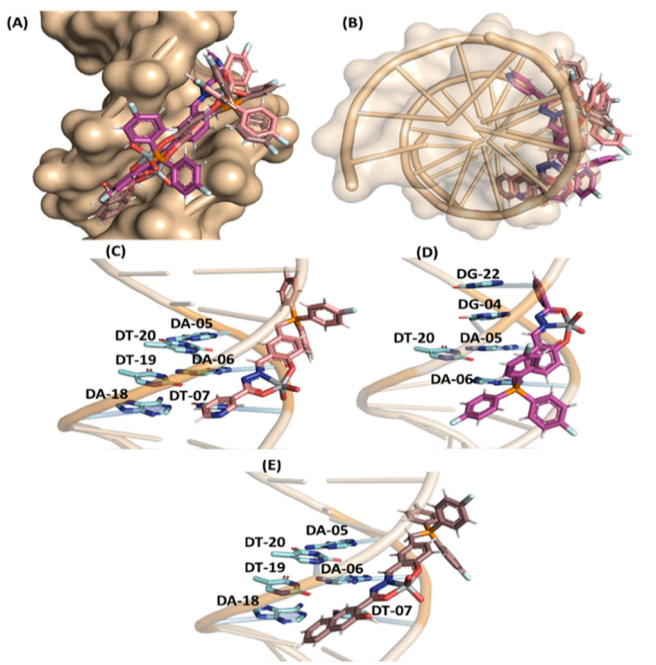

Fig. 6 Superposition of the best docking pose for the interaction DNA:$[V^{V}O_2]$–complexes in the minor groove as the (A) front view and (B) top view. A zoom representation for the interaction: (C) DNA:**C1**, (D) DNA:**C2**, and (E) DNA:**C3**. Selected nucleobases, **C1**, **C2**, and **C3,** are in stick representation in light blue, beige, pink, and brown, respectively. Elements' color: hydrogen, oxygen, nitrogen, fluorine, phosphorus, and vanadium(v) are in white, red, dark blue, cyan, orange, and gray, respectively. For better interpretation, the hydrogen atoms from nucleobases were omitted.

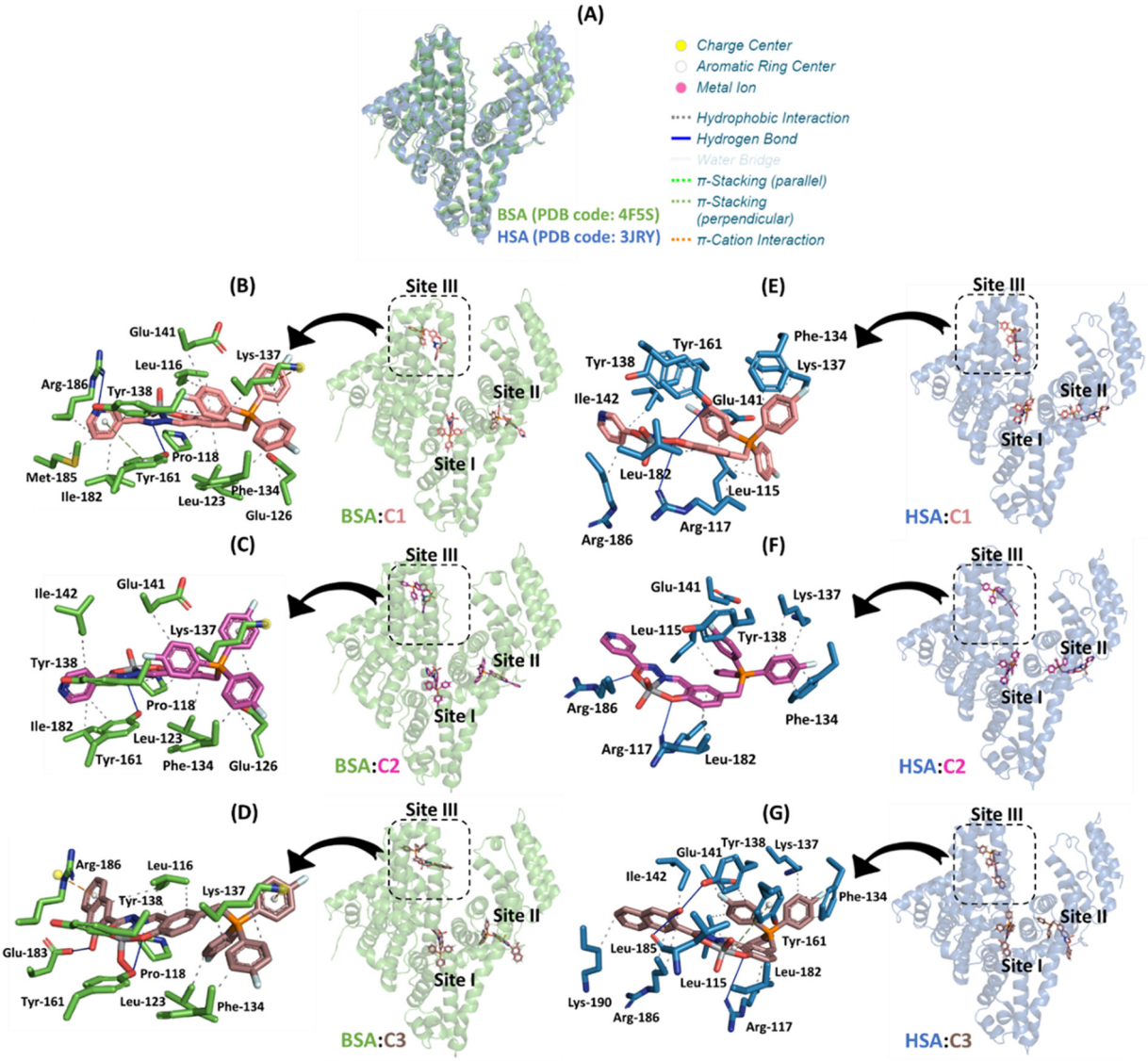

Fig. 7 (A) Superposition of the 3D structures of BSA and HSA (PDB codes 4F5S and 3JRY, respectively). The best docking pose for the interaction: (B) BSA:**C1**, (C) BSA:**C2**, (D) BSA:**C3**, (E) HSA:**C1**, (F) HSA:**C2**, and (G) HSA:**C3** in the three main binding sites with a zoom representation for subdomain IB. Selected amino acid residues for BSA and HSA, **C1**, **C2**, and **C3**, are in stick representation in green, duck blue, beige, pink, and brown, respectively. Elements' color: oxygen, nitrogen, fluorine, phosphorus, and vanadium(v) are in red, dark blue, cyan, orange, and gray, respectively. For better interpretation, all hydrogen atoms were omitted.

hydrogen bonding and/or hydrophobic interactions with the protein surface, corroborating with the data described above. Finally, *in silico* calculations suggested that the naphthalenol moiety of **C3** is more buried into the protein cavity than the nicotinic and isonicotinic moieties of **C1** and **C2**, respectively, reinforcing the obtained highest experimental binding capacity for **C3** to albumin.

Both experimental and *in silico* results indicated that the chemical nature of the pendant arms impacts not only the binding capacity to the biomacromolecules but also the steady-state fluorescence signal. For example, for **C1**, the isosbestic point detected an exciplex formation in the presence of albumin (Fig. 5). Molecular docking calculations suggested that it occurs due to the capacity of the nicotinic moiety from **C1** to interact with the fluorophore Tyr-161 *via* π-stacking force (Fig. 7B). In other words, since albumin was excited at 280 nm, the amino acid residue Tyr in its excited state might transfer energy to the nicotinic moiety of **C1**. In the case of **C2** and **C3**, a weak and non-exciplex formation was detected, respectively (Fig. S61 and Fig. 5B, respectively). The *in silico* results suggested that the isonicotinic and naphthalenol moieties from **C2** and **C3**, respectively, interact differently in the subdomain IB of albumin, *i.e.*, the isonicotinic moiety interacts with Tyr-161 *via* hydrophobic forces (Fig. 7C). In contrast, naphthalenol does not interact with aromatic amino acid residues (Fig. 7D).

Finally, despite the number of connecting points for BSA-**C3** is lower than that for BSA-**C1** and BSA-**C2** (Fig. 7), the inorganic complex **C3** presented the highest binding affinity (around 6- and 4.7-fold higher than **C1** and **C2**, respectively, Table 2) probably due to the capacity of the naphthalenol moiety in interaction *via* π-cation forces with the charge center of Arg-186 driven by the hydrogen bond between the hydroxyl group of the naphthalenol moiety and Glu-183.

Conclusions

In this work, we successfully synthetized three novel vanadium complexes (**C1–C3**) derived from three iminic ligands (**[H_2L1]Cl**–**[H_3L3]Cl**) containing a tris(4-fluorophenyl)phosphonium (**[AF]Cl**) moiety. The complexes, obtained as single-crystals, had their solid-state structure elucidated by the single-crystal X-ray diffraction technique, revealing **C1–C3** as *cis*-dioxidovanadium(v) zwitterionic complexes. The structures of the complexes were also corroborated by several solid-state and solution characterization techniques.

In vitro tests with DNA revealed that complexes **C1–C3** are capable of interacting with and cleaving DNA. Competitive binding studies combined with *in silico* modeling indicated a preference for all the complexes to bind to the minor groove of DNA, significant for the specificity of DNA cleavage. All the new vanadium(v) compounds exhibited significant interactions with the protein, as demonstrated by the binding constant values from emission spectroscopy, indicating a substantial interaction between BSA and the complexes.

Experimental and molecular docking studies showed that compound **C3**, which incorporates naphthalenol as a pendant arm on the ligand, interacts more strongly with the protein than **C1** and **C2**. This heightened interaction is attributed to π-stacking, enhancing the attraction between the amino acid (the naphthalenol moiety of **C3** is more buried into the protein cavity than the nicotinic and isonicotinic moieties of **C1** and **C2**, respectively) residues and the compound.

Author contributions

Francisco Mainardi Martins: methodology, formal analysis, investigation, writing – original draft, writing – review and editing, and visualization. Daniele Cocco Durigon: methodology, formal analysis, investigation, writing – original draft, writing – review and editing, and visualization. Otávio Augusto Chaves: software, validation, investigation, writing – original draft, writing – review and editing, and visualization. Rosely Aparecida Peralta: formal analysis, investigation, writing – review and editing, and visualization. Davi Fernando Back: methodology, validation, formal analysis, investigation, writing – original draft, writing – review and editing, visualization, supervision, and funding acquisition. Hernán Terenzi: methodology, validation, formal analysis, investigation, writing – original draft, writing – review and editing, visualization, supervision, project administration, and funding acquisition.

Data availability

The authors confirm that the data supporting the findings of this study are available within the article and its ESI.† CCDC 2367124, 2367125, and 2367126 contain the supplementary crystallographic data for complexes **C1–C3**, respectively.†

Conflicts of interest

There are no conflicts to declare.

Acknowledgements

The authors thank the Laboratório de Biologia Molecular Estrutural (LABIME) from Universidade Federal de Santa Catarina (UFSC) for ESI-MS analysis and would like to thank the financial agencies: Brazilian Research Councils: CNPq – Edital PQ 308411/2022-6 and CAPES-PROEX – Finance Code 001. We would also like to thank Atlas Assessoria Linguística for support with the English version of this manuscript. O. A. C. also thanks Fundação para a Ciência e Tecnologia (FCT, Portuguese agency for scientific research) for his PhD fellowship 2020.07504.BD (**https://doi.org/10.54499/2020.07504.BD**).

Notes and references

1 C. Metcalfe and J. A. Thomas, *Chem. Soc. Rev.*, 2003, **32**, 215.
2 R. Oun, Y. E. Moussa and N. J. Wheate, *Dalton Trans.*, 2018, **47**, 6645–6653.
3 A. Callejo, L. Sedó-Cabezón, I. Juan and J. Llorens, *Toxics*, 2015, **3**, 268–293.
4 L. Galluzzi, I. Vitale, J. Michels, C. Brenner, G. Szabadkai, A. Harel-Bellan, M. Castedo and G. Kroemer, *Cell Death Dis.*, 2014, **5**, e1257.
5 L. Galluzzi, L. Senovilla, I. Vitale, J. Michels, I. Martins, O. Kepp, M. Castedo and G. Kroemer, *Oncogene*, 2012, **31**, 1869–1883.
6 B. K. Biswas, N. Biswas, S. Saha, A. Rahaman, D. P. Mandal, S. Bhattacharjee, N. Sepay, E. Zangrando, E. Garribba and C. Roy Choudhury, *J. Inorg. Biochem.*, 2022, **237**, 111980.
7 A. Kellett, Z. Molphy, C. Slator, V. McKee and N. P. Farrell, *Chem. Soc. Rev.*, 2019, **48**, 971–988.
8 B. J. Pages, D. L. Ang, E. P. Wright and J. R. Aldrich-Wright, *Dalton Trans.*, 2015, **44**, 3505–3526.
9 C. Wende, C. Lüdtke and N. Kulak, *Eur. J. Inorg. Chem.*, 2014, 2597–2612.
10 E. Palmajumder, S. R. Dash, J. Mitra and K. K. Mukherjea, *ChemistrySelect*, 2018, **3**, 7429–7438.
11 E. Palmajumder, N. Sepay and K. K. Mukherjea, *J. Biomol. Struct. Dyn.*, 2018, **36**, 919–927.
12 Z. Yu and J. Cowan, *Curr. Opin. Chem. Biol.*, 2018, **43**, 37–42.
13 M. Anjomshoa and B. Amirheidari, *Coord. Chem. Rev.*, 2022, **458**, 214417.

14 I. Correia, S. Roy, C. P. Matos, S. Borovic, N. Butenko, I. Cavaco, F. Marques, J. Lorenzo, A. Rodríguez, V. Moreno and J. C. Pessoa, *J. Inorg. Biochem.*, 2015, **147**, 134–146.
15 L. Shi, Y.-Y. Jiang, T. Jiang, W. Yin, J.-P. Yang, M.-L. Cao, Y.-Q. Fang and H.-Y. Liu, *Molecules*, 2017, **22**, 1084.
16 D. Li, N. Zhang, Z. Yang and Z. Tao, *Appl. Organomet. Chem.*, 2017, **31**, e3548.
17 M. Ganeshpandian, M. Palaniandavar, A. Murugananthan, S. K. Ghosh, A. Riyasdeen and M. A. Akbarsha, *Appl. Organomet. Chem.*, 2018, **32**, e4154.
18 S. Akhter, M. Usman, F. Arjmand and S. Tabassum, *Polyhedron*, 2022, **213**, 115618.
19 P. R. Inamdar and A. Sheela, *Int. J. Biol. Macromol.*, 2015, **76**, 269–278.
20 R. Paulpandiyan and N. Raman, *Bioorg. Chem.*, 2017, **73**, 100–108.
21 E. K. Moore, J. Hao, S. J. Spielman and N. Yee, *Geobiology*, 2020, **18**, 127–138.
22 K. Kustin, *J. Inorg. Biochem.*, 2015, **147**, 32–38.
23 L. Hernández, M. L. Araujo, W. Madden, E. Del Carpio, V. Lubes and G. Lubes, *J. Inorg. Biochem.*, 2022, **229**, 111712.
24 S. M. Shaheen, D. S. Alessi, F. M. G. Tack, Y. S. Ok, K.-H. Kim, J. P. Gustafsson, D. L. Sparks and J. Rinklebe, *Adv. Colloid Interface Sci.*, 2019, **265**, 1–13.
25 M. Sutradhar, J. A. L. Da Silva and A. J. L. Pombeiro, in *Vanadium Catalysis*, ed. M. Sutradhar, A. J. L. Pombeiro and J. A. L. Da Silva, The Royal Society of Chemistry, 2020, pp. 1–11.
26 G. Sahu, A. Banerjee, R. Samanta, M. Mohanty, S. Lima, E. R. T. Tiekink and R. Dinda, *Inorg. Chem.*, 2021, **60**, 15291–15309.
27 D. Rehder, *Metallomics*, 2015, **7**, 730–742.
28 D. Rehder, *Inorg. Chim. Acta*, 2023, **549**, 121387.
29 J. Costa Pessoa, E. Garribba, M. F. A. Santos and T. Santos-Silva, *Coord. Chem. Rev.*, 2015, **301–302**, 49–86.
30 L. C. Seefeldt, Z.-Y. Yang, D. A. Lukoyanov, D. F. Harris, D. R. Dean, S. Raugei and B. M. Hoffman, *Chem. Rev.*, 2020, **120**, 5082–5106.
31 N. S. Sickerman, Y. Hu and M. W. Ribbe, *Chem. - Asian J.*, 2017, **12**, 1985–1996.
32 Z. Chen, *Coord. Chem. Rev.*, 2022, **457**, 214404.
33 C. C. McLauchlan, H. A. Murakami, C. A. Wallace and D. C. Crans, *J. Inorg. Biochem.*, 2018, **186**, 267–279.
34 A. A. Sharfalddin, I. M. Al-Younis, H. A. Mohammed, M. Dhahri, F. Mouffouk, H. Abu Ali, Md. J. Anwar, K. A. Qureshi, M. A. Hussien, M. Alghrably, M. Jaremko, N. Alasmael, J. I. Lachowicz and A.-H. Emwas, *Inorganics*, 2022, **10**, 244.
35 G. Sahu, E. R. T. Tiekink and R. Dinda, *Inorganics*, 2021, **9**, 66.
36 J. C. Pessoa, S. Etcheverry and D. Gambino, *Coord. Chem. Rev.*, 2015, **301–302**, 24–48.
37 S. Treviño and A. Diaz, *J. Inorg. Biochem.*, 2020, **208**, 111094.
38 J. H. McNeill, V. G. Yuen, H. R. Hoveyda and C. Orvig, *J. Med. Chem.*, 1992, **35**, 1489–1491.
39 K. H. Thompson and C. Orvig, *J. Inorg. Biochem.*, 2006, **100**, 1925–1935.
40 A. Sinha, R. Chaudhary, D. S. Reddy, M. Kongot, M. M. Kurjogi and A. Kumar, *Heliyon*, 2022, **8**, e10125.
41 N. Samart, Z. Arhouma, S. Kumar, H. A. Murakami, D. C. Crick and D. C. Crans, *Front. Chem.*, 2018, **6**, 519.
42 A. Zahirović, B. Tüzün, S. Hadžalić, I. Osmanković, S. Roca, S. Begić and M. Fočak, *J. Mol. Struct.*, 2023, **1294**, 136564.
43 S. Semiz, *J. Trace Elem. Med. Biol.*, 2022, **69**, 126887.
44 S.-Y. Wong, R. Wai-Yin Sun, N. P.-Y. Chung, C.-L. Lin and C.-M. Che, *Chem. Commun.*, 2005, 3544.
45 M. F. Mosquillo, P. Smircich, A. Lima, S. A. Gehrke, G. Scalese, I. Machado, D. Gambino, B. Garat and L. Pérez-Díaz, *Bioinorg. Chem. Appl.*, 2020, **2020**, 1–10.
46 B. Casarrubias-Tabarez, N. Rivera-Fernández, M. Rojas-Lemus, N. López-Valdez and T. I. Fortoul, *Toxicol. Rep.*, 2020, **7**, 1001–1007.
47 I. Leon, J. Cadavid-Vargas, A. Di Virgilio and S. Etcheverry, *Curr. Med. Chem.*, 2017, **24**, 112–148.
48 S. Kumar, S. Kumari, R. Karan, A. Kumar, R. K. Rawal and P. Kumar Gupta, *Inorg. Chem. Commun.*, 2024, **161**, 112014.
49 C. Amante, A. L. De Sousa-Coelho and M. Aureliano, *Metals*, 2021, **11**, 828.
50 O. J. D'Cruz and F. M. Uckun, *Expert Opin. Invest. Drugs*, 2002, **11**, 1829–1836.
51 S. P. Dash, A. K. Panda, S. Dhaka, S. Pasayat, A. Biswas, M. R. Maurya, P. K. Majhi, A. Crochet and R. Dinda, *Dalton Trans.*, 2016, **45**, 18292–18307.
52 L. P. Fioravanço, J. B. Pôrto, F. M. Martins, J. D. Siqueira, B. A. Iglesias, B. M. Rodrigues, O. A. Chaves and D. F. Back, *J. Inorg. Biochem.*, 2023, **239**, 112070.
53 D. Patra, N. Biswas, B. Kumari, P. Das, N. Sepay, S. Chatterjee, M. G. B. Drew and T. Ghosh, *RSC Adv.*, 2015, **5**, 92456–92472.
54 S. Saswati, P. Adão, S. Majumder, S. P. Dash, S. Roy, M. L. Kuznetsov, J. Costa Pessoa, C. S. B. Gomes, M. R. Hardikar, E. R. T. Tiekink and R. Dinda, *Dalton Trans.*, 2018, **47**, 11358–11374.
55 L. Mato-López, A. Sar-Rañó, M. R. Fernández, M. L. Díaz-Prado, A. Gil, Á. Sánchez-González, N. Fernández-Bertólez, J. Méndez, V. Valdiglesias and F. Avecilla, *J. Inorg. Biochem.*, 2022, **235**, 111937.
56 G. Sahu, S. A. Patra, P. D. Pattanayak, W. Kaminsky and R. Dinda, *Inorg. Chem.*, 2023, **62**, 6722–6739.
57 S. P. Dash, A. K. Panda, S. Pasayat, R. Dinda, A. Biswas, E. R. T. Tiekink, S. Mukhopadhyay, S. K. Bhutia, W. Kaminsky and E. Sinn, *RSC Adv.*, 2015, **5**, 51852–51867.
58 S. P. Dash, A. K. Panda, S. Pasayat, R. Dinda, A. Biswas, E. R. T. Tiekink, Y. P. Patil, M. Nethaji, W. Kaminsky, S. Mukhopadhyay and S. K. Bhutia, *Dalton Trans.*, 2014, **43**, 10139.
59 S. P. Dash, A. K. Panda, S. Pasayat, S. Majumder, A. Biswas, W. Kaminsky, S. Mukhopadhyay, S. K. Bhutia and R. Dinda, *J. Inorg. Biochem.*, 2015, **144**, 1–12.
60 A. Kumar, I. Pant, A. Dixit, S. Banerjee, B. Banik, R. Saha, P. Kondaiah and A. R. Chakravarty, *J. Inorg. Biochem.*, 2017, **174**, 45–54.

61 P. Lu, B. J. Bruno, M. Rabenau and C. S. Lim, *J. Controlled Release*, 2016, **240**, 38–51.
62 W. Xu, Z. Zeng, J. Jiang, Y. Chang and L. Yuan, *Angew. Chem., Int. Ed.*, 2016, **55**, 13658–13699.
63 G. Schanne, L. Henry, H. C. Ong, A. Somogyi, K. Medjoubi, N. Delsuc, C. Policar, F. García and H. C. Bertrand, *Inorg. Chem. Front.*, 2021, **8**, 3905–3915.
64 S. Purser, P. R. Moore, S. Swallow and V. Gouverneur, *Chem. Soc. Rev.*, 2008, **37**, 320–330.
65 R. Guo and J. Chen, *RSC Adv.*, 2018, **8**, 17110–17120.
66 E. A. Ilardi, E. Vitaku and J. T. Njardarson, *J. Med. Chem.*, 2014, **57**, 2832–2842.
67 M. Strohalm, D. Kavan, P. Novák, M. Volný and V. Havlíček, *Anal. Chem.*, 2010, **82**, 4648–4651.
68 G. M. Sheldrick, *Acta Crystallogr., Sect. A: Found. Crystallogr.*, 2008, **64**, 112–122.
69 L. J. Farrugia, *J. Appl. Crystallogr.*, 1997, **30**, 565.
70 L. J. Farrugia, *J. Appl. Crystallogr.*, 2012, **45**, 849–854.
71 Y. Jin, M. A. Lewis, N. H. Gokhale, E. C. Long and J. A. Cowan, *J. Am. Chem. Soc.*, 2007, **129**, 8353–8361.
72 H. R. Drew, R. M. Wing, T. Takano, C. Broka, S. Tanaka, K. Itakura and R. E. Dickerson, *Proc. Natl. Acad. Sci. U. S. A.*, 1981, **78**, 2179–2183.
73 A. Bujacz, *Acta Crystallogr., Sect. D: Biol. Crystallogr.*, 2012, **68**, 1278–1289.
74 K. L. Hein, U. Kragh-Hansen, J. P. Morth, M. D. Jeppesen, D. Otzen, J. V. Møller and P. Nissen, *J. Struct. Biol.*, 2010, **171**, 353–360.
75 T. Bessega, O. A. Chaves, F. M. Martins, T. V. Acunha, D. F. Back, B. A. Iglesias and G. M. De Oliveira, *Inorg. Chim. Acta*, 2019, **496**, 119049.
76 O. A. Chaves, M. R. De Lima Santos, M. C. C. De Oliveira, C. M. R. Sant'Anna, R. C. Ferreira, A. Echevarria and J. C. Netto-Ferreira, *J. Mol. Liq.*, 2018, **254**, 280–290.
77 O. A. Chaves, D. Cesarin-Sobrinho, C. M. R. Sant'Anna, M. G. De Carvalho, L. R. Suzart, F. E. A. Catunda-Junior, J. C. Netto-Ferreira and A. B. B. Ferreira, *J. Photochem. Photobiol., A*, 2017, **336**, 32–41.
78 M. F. Adasme, K. L. Linnemann, S. N. Bolz, F. Kaiser, S. Salentin, V. J. Haupt and M. Schroeder, *Nucleic Acids Res.*, 2021, **49**, W530–W534.
79 S. Yuan, H. C. S. Chan and Z. Hu, *Wiley Interdiscip. Rev.: Comput. Mol. Sci.*, 2017, **7**, e1298.
80 S. A. Aboafia, S. A. Elsayed, A. K. A. El-Sayed and A. M. El-Hendawy, *J. Mol. Struct.*, 2018, **1158**, 39–50.
81 W. Henderson, L. L. Koh, J. D. Ranford, W. T. Robinson, J. O. Svensson, J. J. Vittal, Y. M. Wang and Y. Xu, *J. Chem. Soc., Dalton Trans.*, 1999, 3341–3343.
82 S. D. Kurbah, M. Asthana, I. Syiemlieh, A. A. Lywait, M. Longchar and R. A. Lal, *J. Organomet. Chem.*, 2018, **876**, 10–16.
83 M. Mohanty, S. K. Maurya, A. Banerjee, S. A. Patra, M. R. Maurya, A. Crochet, K. Brzezinski and R. Dinda, *New J. Chem.*, 2019, **43**, 17680–17695.
84 A. W. Addison, T. N. Rao, J. Reedijk, J. Van Rijn and G. C. Verschoor, *J. Chem. Soc., Dalton Trans.*, 1984, 1349–1356.
85 M. Sutradhar and A. J. L. Pombeiro, *Coord. Chem. Rev.*, 2014, **265**, 89–124.
86 M. R. Maurya, C. Haldar, A. Kumar, M. L. Kuznetsov, F. Avecilla and J. Costa Pessoa, *Dalton Trans.*, 2013, **42**, 11941.
87 M. R. Maurya, N. Jangra, F. Avecilla, N. Ribeiro and I. Correia, *ChemistrySelect*, 2019, **4**, 12743–12756.
88 R. Borah, S. Lahkar, N. Deori and S. Brahma, *RSC Adv.*, 2022, **12**, 13740–13748.
89 R. Borah, N. Deori, S. Lahkar, S. Paul and S. Brahma, *J. Mol. Struct.*, 2023, **1293**, 136224.
90 S. Thakur, S. Wahedur, R. M. Gomila, A. Frontera and S. Chattopadhyay, *Polyhedron*, 2023, **235**, 116335.
91 M. Sirajuddin, S. Ali and A. Badshah, *J. Photochem. Photobiol., B*, 2013, **124**, 1–19.
92 F. Kratz, *J. Controlled Release*, 2008, **132**, 171–183.
93 S. Ketrat, D. Japrung and P. Pongprayoon, *J. Mol. Graphics Modell.*, 2020, **98**, 107601.
94 N. J. Turro, V. Ramamurthy and J. C. Scaiano, *Principles of molecular photochemistry: an introduction*, University Science Books, Sausalito, Calif, 1st edn, 2009.
95 G. F. Rio, L. H. E. Castro, G. S. R. Souza, O. Augusto Chaves, M. Edilson Freire De Lima, D. Cesarin-Sobrinho and C. M. R. Sant'Anna, *J. Mol. Liq.*, 2024, **407**, 125247.
96 O. A. Chaves, R. J. S. Loureiro, C. Serpa, P. F. Cruz, A. B. B. Ferreira and J. C. Netto-Ferreira, *Int. J. Biol. Macromol.*, 2024, **263**, 130279.
97 F. M. Martins, B. A. Iglesias, O. A. Chaves, J. L. Gutknecht Da Silva, D. B. R. Leal and D. F. Back, *Dalton Trans.*, 2024, **53**, 8315–8327.
98 M. Montalti, A. Credi, L. Prodi and M. T. Gandolfi, *Handbook of Photochemistry*, CRC Press, Boca Raton, FL, USA, 3rd edn, 2006.
99 M. A. G. Soares, F. Souza-Silva, C. R. Alves, L. Vazquez, T. S. De Araujo, C. Serpa and O. A. Chaves, *Sci. Pharm.*, 2024, **92**, 32.
100 T. V. Acunha, B. M. Rodrigues, J. A. Da Silva, D. D. M. Galindo, O. A. Chaves, V. N. Da Rocha, P. C. Piquini, M. H. Köhler, L. De Boni and B. A. Iglesias, *J. Mol. Liq.*, 2021, **340**, 117223.
101 O. A. Chaves, C. S. H. Jesus, P. F. Cruz, C. M. R. Sant'Anna, R. M. M. Brito and C. Serpa, *Spectrochim. Acta, Part A*, 2016, **169**, 175–181.
102 V. S. Câmara, O. A. Chaves, B. B. De Araújo, P. F. B. Gonçalves, B. A. Iglesias, M. A. Ceschi and F. S. Rodembusch, *J. Mol. Liq.*, 2022, **349**, 118084.
103 O. A. Chaves, M. C. C. De Oliveira, C. M. C. De Salles, F. M. Martins, B. A. Iglesias and D. F. Back, *J. Inorg. Biochem.*, 2019, **200**, 110800.
104 D. M. Dias, J. P. G. L. M. Rodrigues, N. S. Domingues, A. M. J. J. Bonvin and M. M. C. A. Castro, *Eur. J. Inorg. Chem.*, 2013, 4619–4627.